

Local Map-assisted Positioning for Flying Wireless Relays

Junting Chen, *Member, IEEE*, and David Gesbert, *Fellow, IEEE*

Abstract—This paper considers the exploitation of unmanned aerial vehicles (UAVs) in wireless networking, with which communication-enabled robots operate as flying wireless relays to provide connectivity or a capacity boost to a ground user. We focus on the particular problem of (automatic) UAV positioning, which greatly affects the end-to-end throughput performance. While existing methods rely on propagation distance minimization and statistical models for the presence or absence of a line-of-sight (LOS), we propose an approach capable of leveraging local topological information so as to offer better performance guarantees. The proposed method allows to strike a trade-off between minimizing distance path loss and discovering (near) LOS opportunities at locations away from the base station (BS)-user axis. Furthermore, the algorithm is shown to find the global optimal UAV position, although it only requires a *local* exploration of a signal strength map and the length of search trajectory is only linear to the geographical scale. Hence, it lends itself to online implementation. Significant throughput gains are found when compared to other positioning approaches based on LOS statistical models.

I. INTRODUCTION

The demand for high data rate and low latency wireless service has dramatically increased in recent years. To address the challenge, future wireless communication technologies strive to bring the network infrastructure closer to the user and provide higher bandwidth, *e.g.*, through the deployment of small cells and the application of millimeter-wave. However, a known fundamental challenge is shadowing at the user-side that blocks the signal. Recently, substantial research attention has been brought on the exploitation of UAVs as flying relays with flexible positioning so as to relay the signal from the air for the BS and the user [1]–[7].

However, it is often difficult to find the optimal UAV position for relaying because the shadowing that obstructs the UAV-to-user signal depends on the complex, and usually irregular, urban topology (*e.g.*, buildings and vegetation). Even in the case of relaying to a single user, the resulting optimal UAV position may not simply locate on the BS-user axis.

A. Related Works

One essential issue for positioning the UAV is to predict the air-to-ground channel, since a precise UAV-user channel

knowledge is usually not available before the UAV is sent to a target position. As a way to circumvent this problem, some prior works simply assumed LOS propagation from the UAV to the ground user, and hence the channel gain is merely an explicit continuous function of the UAV position. Using the LOS model, [8]–[11] focused on UAV navigation problems, and [12] studied the multiple-input multiple-output (MIMO) channel to jointly optimize the UAV position and the orientation of a uniform linear antenna array (ULA) mounted at the UAV for the best spatial channel to multiple users. However, LOS models overestimate the channel gain in urban scenarios, especially in low altitude UAV applications, because there the air-to-ground signal is likely blocked by obstacles surrounding the user, and such a user-side shadowing effect significantly dominates the relay performance.

To capture the shadowing effect, the works [13]–[17] studied a stochastic LOS model, which computes an empirical LOS probability as a function of the elevation angle from the user to the UAV. Such a model captures the practical experience that the larger the elevation angle, the higher chance to see LOS propagation from the air to the ground. With that, the works [13]–[17], for instance, optimized the UAV position to maximize the UAV signal coverage and minimize the UAV power consumption. However, *macroscopic* LOS statistics fails to capture the fine-grained propagation pattern due to the urban topology, and hence those approaches [13]–[17] can only be suboptimal.

B. Challenges and Contributions

In reality, the obstacle distribution depends on a specific user location and is *not* homogeneous with respect to (w.r.t.) another user location. As a result, the air-to-ground channel gain depends on not only the UAV-user distance, but also the local terrain. In a scenario such as a UAV flying over a building that originally shadowed a user, a slight change of the UAV position may result in a significant change in the air-to-ground channel gain (for example, when the UAV just leaves the shadow). Ideally, optimal UAV positioning may require a fully detailed air-to-ground propagation database, but such a brute-force strategy results in an overwhelming complexity.

The goal of this paper is to adapt the UAV relay system to the geographically fine-grained propagation environment, by developing a low complexity trajectory for the UAV to explore for the optimal relay position from the air. Specifically, two fundamental challenges are to be addressed:

- **How to model a fine-grained air-to-ground propagation channel?** We need a model that not only captures

This work was supported by the ERC under the European Union Horizon 2020 research and innovation program (Agreement no. 670896).

J. Chen was with the Department of Communication Systems, EURECOM, France. He is now with the Ming Hsieh Department of Electrical Engineering, University of Southern California, Los Angeles, CA 90089, USA (email: juntincg@usc.edu). D. Gesbert is with the Department of Communication Systems, EURECOM, France (email: gesbert@eurecom.fr).

the user-side non-parametric shadowing information but also facilitates low complexity algorithm for optimal UAV positioning.

- **How to plan an efficient search trajectory for the optimal UAV position?** It is not feasible to explore the entire target area for the optimal UAV position due to the practical constraint on the UAV flight time. Therefore, it is critical to plan for an intelligent UAV trajectory with a limited path length for the search.

In this paper, we propose a *nested segmented* air-to-ground propagation model, which captures two important propagation properties that are previously observed and leveraged in prior works [18] and [13], respectively: First, the UAV location space can be partitioned into propagation segments depending on the degree of obstruction of the UAV-user link, such as pure LOS, lightly obstructed LOS, and non-line-of-sight (NLOS) conditions [18]. Second, as the UAV moves away from the ground user, the UAV-user link tends to experience gradually worsening shadowing, *e.g.*, from pure LOS to strongly obstructed NLOS [13]. We establish a mathematical model for the nested segmented propagation property and show that such a model can be leveraged for *globally* optimal UAV positioning *without* the need of a *global* radio map exploration. While this idea was partially exploited in our preliminary work [19], the work [19] focused only on the simplest case of two propagation segments.

To summarize, the key contributions are made as follows:

- We propose a nested segmented propagation model for the air-to-ground channel and develop an algorithm framework to search for the optimal position for UAV relaying.
- We establish theoretical results to prove that the proposed algorithm finds the global optimal UAV position in a relay system for a BS and a user, while the length of the search trajectory is only linear to the BS-user distance; a global exploration is *not* needed.
- We perform numerical experiments to evaluate the end-to-end throughput and compare with existing approaches based on stochastic LOS models and an intuitive baseline that limits the search to the BS-user axis. Throughput gains of up to 300% are found based on Monte Carlo analysis for an urban Manhattan-like environment.

The rest of the paper is organized as follows. Section II establishes the nested segmented air-to-ground propagation model. Section III develops the search algorithm from the two propagation segment case to the case of arbitrary number of segments. Section IV establishes theoretical results on the global optimality. Numerical results are demonstrated in Section V, and conclusions are given in Section VI.

II. SYSTEM MODEL

Consider a cellular network in a dense urban environment, where the direct BS-to-user transmission is obstructed by obstacles such as buildings or trees. A UAV flies with a fixed altitude H_D in the air to relay the signal between the BS and the user. Denote $\mathbf{x} \in \mathbb{R}^2$ as the position of the UAV to be

optimized, and $\tilde{\mathbf{x}} = (\mathbf{x}, H_d) \in \mathbb{R}^3$ as the corresponding UAV position in 3D space.

We consider that the altitudes H_b of the BS and H_d of the UAV are large enough such that there is *always* LOS propagation between the BS and the UAV. We define the *channel* as the deterministic power gain averaged over small scale fading. The BS-UAV channel is modeled as

$$g_b(\mathbf{x}) = \beta_0 d_b(\mathbf{x})^{-\alpha_0} \quad (1)$$

where $d_b(\mathbf{x}) = \sqrt{\|\mathbf{x} - \mathbf{x}_b\|^2 + (H_d - H_b)^2}$ is the distance from the UAV at (\mathbf{x}, H_d) to the BS at (\mathbf{x}_b, H_b) , and the constants $\alpha_0 > 1$ and $\beta_0 > 0$ are the classical path loss exponent and offset parameters.

A. Nested Segmented Air-to-ground Propagation Model

We consider a *nested segmented* propagation structure to model the various degrees of shadowing for the air-to-ground channel. Specifically, let $\mathbb{D} \subseteq \mathbb{R}^2$ be the domain of all possible UAV positions \mathbf{x} at constant altitude H_d . Consider a partition of \mathbb{D} into K disjoint segments according to the *actual* propagation environment around user position $\tilde{\mathbf{x}}_u \in \mathbb{R}^3$, *i.e.*, $\mathbb{D} = \mathcal{D}_1(\tilde{\mathbf{x}}_u) \cup \mathcal{D}_2(\tilde{\mathbf{x}}_u) \cup \dots \cup \mathcal{D}_K(\tilde{\mathbf{x}}_u)$, where $\mathcal{D}_k \cap \mathcal{D}_j = \emptyset$, for $k \neq j$, and $\mathcal{D}_k(\tilde{\mathbf{x}}_u)$ denotes the region of UAV locations for which the UAV maintains a degree- k of LOS obstruction. The notion of degree is further detailed below through the UAV-user channel:

$$g_u(\mathbf{x}) = \sum_{k=1}^K \beta_k d_u(\mathbf{x})^{-\alpha_k} \mathbb{I}\{\mathbf{x} \in \mathcal{D}_k\} \quad (2)$$

where $d_u(\mathbf{x}) = \sqrt{\|\mathbf{x} - \mathbf{x}_u\|^2 + (H_d - H_u)^2}$ is the distance from the UAV located at (\mathbf{x}, H_d) to the user at $\tilde{\mathbf{x}}_u = (\mathbf{x}_u, H_u)$, $\alpha_k > 1$, $\beta_k > 0$, and $\mathbb{I}\{A\}$ is an indicator function taking value 1 if condition A is satisfied, and 0 otherwise. In addition, the partition $\{\mathcal{D}_k, k = 1, 2, \dots, K\}$ is assumed to satisfy the following two conditions: (i) the propagation segment \mathcal{D}_k exhibits a higher degree of LOS obstruction than \mathcal{D}_{k-1} , *i.e.*,

$$\beta_k d_u(\mathbf{x})^{-\alpha_k} < \beta_{k-1} d_u(\mathbf{x})^{-\alpha_{k-1}} \quad (3)$$

for $k = 2, 3, \dots, K$ and any UAV position \mathbf{x} , and (ii) the propagation segments \mathcal{D}_k are nested along any directions from the user, *i.e.*, for any $\mathbf{x} \in \mathcal{D}_k$ and $0 \leq \rho \leq 1$,

$$\mathbf{x}_u + \rho(\mathbf{x} - \mathbf{x}_u) \in \mathcal{D}_j, \quad \text{for some } j \leq k. \quad (4)$$

In other words, when the UAV moves straight towards the user, the UAV-user channel tends to become *always* less obstructed [20].

The nested segmented propagation model (2)–(4) is motivated by the following two observations from typical real-life situations. First, it is a generalization of the classical path loss model (1) to the case of multiple NLOS levels [18], *e.g.*, from light obstruction forms (wood walls) to severe ones (multiple walls). Second, when the UAV moves straight towards the user, it has a higher chance to see less obstructed propagation to the user (as there are fewer obstacles between the UAV and the

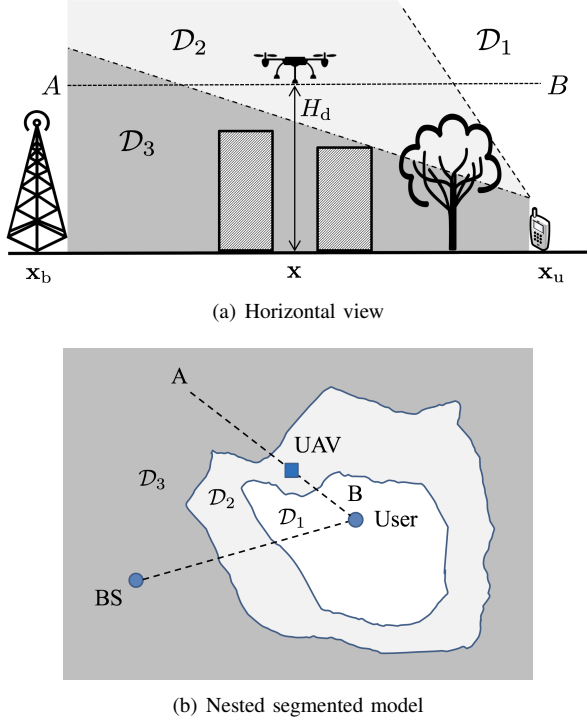


Figure 1. A geometric interpretation of the nested segmented model from (a) horizontal view and (b) top view.

user as the UAV moves closer).¹ Such an observation was also exploited in the stochastic LOS model [13]–[17]. A geometric interpretation is illustrated in Fig. 1.

In this paper, we assume that the number of segments K and the parameters α_k and β_k are known or previously estimated [21], [22]. However, the global knowledge of the propagation segments \mathcal{D}_k is *not* available, and the UAV needs to plan a trajectory to determine $\mathbb{I}\{\mathbf{x} \in \mathcal{D}_k\}$ in (2) along its flight path.

B. Optimal UAV Positioning

Consider a cost function $f(g_u, g_b)$ of the UAV-user channel gain g_u and the BS-UAV channel gain g_b . Assume that $f(x, y)$ is a continuous and decreasing function in x and y , respectively, i.e., $\partial f(x, y)/\partial x$ and $\partial f(x, y)/\partial y$ are negative for all $x, y > 0$ wherever the derivatives exist. Before considering concrete examples, a generic UAV positioning problem can be formulated as follows

$$\mathcal{P}: \quad \underset{\mathbf{x} \in \mathbb{R}^2}{\text{minimize}} \quad f(g_u(\mathbf{x}), g_b(\mathbf{x})).$$

The difficulty in solving \mathcal{P} is twofold: First, the function $g_u(\mathbf{x})$ is segmented according to the urban topology. Secondly, $f(g_u(\mathbf{x}), g_b(\mathbf{x}))$ may not be convex in the variable \mathbf{x} . The goal of this paper is to develop efficient algorithms to find the globally optimal solution to \mathcal{P} .

Note that although the formulation \mathcal{P} considers a relay system for a single user U , in practice, the UAV relay can actually provide service to multiple users in a local area

¹We also note that there are some rare cases of exceptions. For example, a building with a big hole located between the UAV and the user may break this assumption.

centered at U , where every user experiences in a similar shadowing environment.

C. Application Examples

The transmission from the BS to the UAV is modeled as $y_r = \sqrt{P_b g_b} a_b s + n_r$, and that from the UAV to the user is modeled as $y_u = \sqrt{P_u g_u} a_u s_r + n_u$, where $n_r, n_u \sim \mathcal{CN}(0, 1)$ are the receive noise at the UAV relay and the user, respectively, $s, s_r \sim \mathcal{N}(0, 1)$ are the transmit signals from the BS and the UAV relay, respectively. The variables a_b and a_u model the small scale fading on the BS-UAV link and the UAV-user link, respectively. For Rayleigh fading channels, $|a_b|^2$ and $|a_u|^2$ are assumed to follow exponential distribution with parameter (normalized as) $\lambda = 1$.

There are a variety of relay strategies in the literature. To motivate problem \mathcal{P} , we illustrate two examples, respectively, on outage probability minimization for amplify-and-forward relaying and capacity maximization for decode-and-forward relaying.

1) *Amplify-and-Forward*: In amplify-and-forward relaying, the UAV relays the information by transmitting $s_r = y_r / \sqrt{P_b g_b |a_r|^2 + 1}$, where the scaling factor $\sqrt{P_b g_b |a_r|^2 + 1}$ is to normalize the transmission power at the UAV to be P_u . It was shown in [23], [24] that the capacity of the relay channel is given by $C_{AF} = \frac{1}{2} \log_2 (1 + q(P_b g_b |a_r|^2, P_u g_u |a_u|^2))$, where $q(x, y) \triangleq xy/(x + y + 1)$ and the parameter $\frac{1}{2}$ is to capture the fact that the information requires two time slots to reach the user. The outage probability with respect to a target data rate R was shown to be [24, Lemma 1]²

$$\mathbb{P}\{C_{AF} < R\} \approx \left(\frac{1}{P_b g_b} + \frac{1}{P_u g_u} \right) (2^{2R} - 1)^2$$

under high SNR, i.e., $P_b g_b, P_u g_u \gg 1$.

To minimize the outage probability of the relay channel, the desired UAV position can be determined as the solution to the following problem:

$$\begin{aligned} \mathcal{P}1: \quad & \underset{\mathbf{x} \in \mathbb{R}^2}{\text{minimize}} \quad f(g_u(\mathbf{x}), g_b(\mathbf{x})) \\ & := \frac{1}{P_u g_u(\mathbf{x})} + \frac{1}{P_b g_b(\mathbf{x})}. \end{aligned} \quad (5)$$

2) *Decode-and-Forward*: In decode-and-forward relaying, the UAV fully decodes the message \hat{s} from the receive signal y_r , and transmits $s_r = \hat{s}$ to the user. The maximum capacity of such a decode-and-forward relay system can be shown to be $C_{DF} = \frac{1}{2} \min\{\log_2(1 + P_b g_b |a_b|^2), \log_2(1 + P_u g_u |a_u|^2)\}$ [24], [25]. Using Jensen's inequality $\mathbb{E}\{C(x)\} \leq C(\mathbb{E}\{x\})$ on a concave function $C(x)$, an upper bound of the ergodic capacity $\mathbb{E}\{C_{DF}\}$ is given by $\frac{1}{2} \min\{\log_2(1 + P_b g_b), \log_2(1 + P_u g_u)\}$. The desired UAV position can be determined by maximizing

²The original problem in [24] considered a diversity scheme that combines the signal from the relay and the signal from the BS. Such a strategy also leads to problem $\mathcal{P}1$ under high signal-to-noise ratio (SNR).

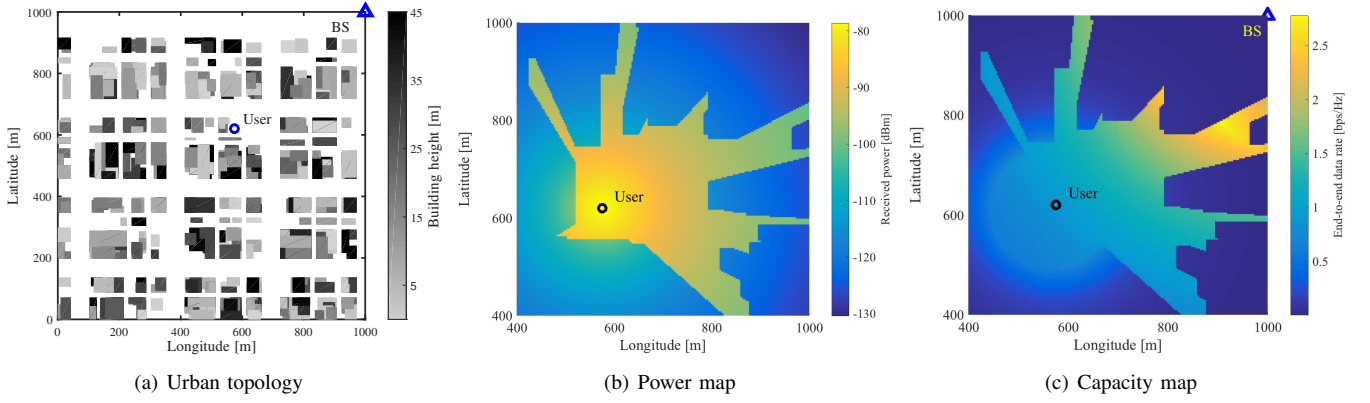


Figure 2. (a) A map of a dense urban area, where the rectangles denote the building with colors representing their heights. (b) The received power map corresponding to every UAV position. (c) The end-to-end capacity map.

such a capacity bound. Equivalently, the problem can be formulated as follows:

$$\begin{aligned} \mathcal{P}2: \quad & \underset{\mathbf{x} \in \mathbb{R}^2}{\text{minimize}} \quad f(g_u(\mathbf{x}), g_b(\mathbf{x})) \\ & := \max \left\{ -\log_2(1 + P_b g_b(\mathbf{x})), \right. \\ & \quad \left. -\log_2(1 + P_u g_u(\mathbf{x})) \right\}. \end{aligned} \quad (6)$$

A numerical example is given in Fig. 2, where Fig. 2 (b) simulates the received power of the UAV-user signal w.r.t. every UAV position under a segmented propagation model with $K = 2$. Fig. 2 (c) shows the corresponding relay channel capacity from the BS to the user via the UAV. It is not trivial to find the optimal UAV relay position due to the irregular propagation pattern.

III. ALGORITHM DESIGNS

In this section, we first derive some useful insights on the optimal UAV positions via a polar representation which better exploits the nested segmented propagation model. Based on that, we develop the search algorithm for the optimal UAV position under two segment case, and then extend to the case of arbitrary number of segments.

A. Properties of the Optimal UAV Position

We first study some generic properties of the solution to \mathcal{P} .

As an intuitive yet naive approach, the optimal UAV position \mathbf{x} could be searched on the BS-user axis so as to simply minimize the total propagation distance. However the area off the BS-user axis may provide opportunities to operate in a better UAV-user propagation segment while moderately increasing the distances. While the complexity of searching the complete area is in principle prohibitive, the result below shows a relatively efficient way of reducing the search space.

Proposition 1. *The optimal solution \mathbf{x}^* to \mathcal{P} is either on the BS-user axis, or on the boundary between two propagation segments.*

Proof. Suppose there is a solution \mathbf{x} which is strictly inside a propagation segment \mathcal{D}_k and is off the BS-user axis. Then

there exists a direction δ , such that for a sufficiently small $\epsilon > 0$, the new UAV position $\mathbf{x} + \epsilon\delta$ decreases the distances to both the user and the BS, and at the same time, $\mathbf{x} + \epsilon\delta \in \mathcal{D}_k$. From the nested segmented model (2) and also the UAV-BS channel model (1), smaller distances d_u and d_b imply larger channel gains g_u and g_b . Due to the monotonicity property of the cost function $f(g_u, g_b)$, larger channel gains yield a smaller cost value, which implies that \mathbf{x} is not the optimal solution. By contradiction, the proposition is therefore confirmed. \square

Proposition 1 suggests an intuitive algorithm that searches along the propagation segment boundaries for the optimal UAV position. However, such an algorithm could be costly to implement, since the segment boundary may have a complex shape, resulting in an unacceptably long trajectory (which could be unbounded even in a bounded two-dimensional search area) for the UAV as demonstrated in Fig. 2.

In what comes below, we circumvent this problem by developing an efficient algorithm that has a limited trajectory length. It turns out that the proposed algorithm does not need to follow the entirety of the propagation boundaries.

B. Polar Representation

To exploit the nested segmented propagation model, we transform the problem into one expressed over a polar coordinate system.

Let $\rho = \|\mathbf{x} - \mathbf{x}_u\|$ be the ground projected distance from the user at (\mathbf{x}_u, H_u) to the UAV at (\mathbf{x}, H_d) . Let $\theta \in (-\pi, \pi)$ be the *deviation angle* from the user-to-BS direction to the user-to-UAV direction as illustrated in Fig. 3. Denote $\mathbf{u} = (u_1, u_2) \triangleq \frac{\mathbf{x}_b - \mathbf{x}_u}{\|\mathbf{x}_b - \mathbf{x}_u\|}$ as the normalized user-to-BS direction. The UAV position $\mathbf{x} \in \mathbb{R}^2$ can be equivalently expressed by (ρ, θ) as

$$\mathbf{x}(\rho, \theta) = \mathbf{x}_u + \rho \mathbf{M}(\theta) \mathbf{u} \quad (7)$$

where

$$\mathbf{M}(\theta) = \begin{bmatrix} \cos \theta & -\sin \theta \\ \sin \theta & \cos \theta \end{bmatrix} \quad (8)$$

is a rotation matrix, and

$$\theta = \text{sign}(z_2 u_1 - z_1 u_2) \cdot \arccos(\mathbf{z}^T \mathbf{u} / \rho) \quad (9)$$

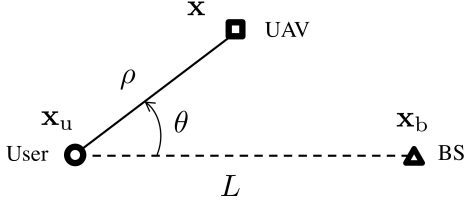


Figure 3. Illustration of a polar representation of the UAV position \mathbf{x} .

in which $\mathbf{z} = (z_1, z_2) \triangleq \mathbf{x} - \mathbf{x}_u$, $\text{sign}(x) = 1$ if $x > 0$, and $\text{sign}(x) = -1$, otherwise.

We now define an alternative expression for the cost function $f(g_u(\mathbf{x}), g_b(\mathbf{x}))$.

Definition 1 (Fictitious Segment Cost Function). For $\mathbf{x}(\rho, \theta) \in \mathcal{D}_k$, $k = 1, 2, \dots, K$, the cost function $f(g_u(\mathbf{x}), g_b(\mathbf{x}))$ can be written as

$$f(g_u(\mathbf{x}), g_b(\mathbf{x})) = F_k(\rho, \theta)$$

where

$$F_k(\rho, \theta) \triangleq f(g_u^{(k)}(\mathbf{x}(\rho, \theta)), g_b(\mathbf{x}(\rho, \theta))) \quad (10)$$

and

$$g_u^{(k)}(\mathbf{x}) \triangleq \beta_k d_u(\mathbf{x})^{-\alpha_k} \quad (11)$$

is the UAV-user channel in the k th segment from the channel model (2).

Note that, due to the nested segmented propagation property (2), $F_{k+1}(\rho, \theta) > F_k(\rho, \theta)$ for $k = 1, 2, \dots, K-1$.

C. Search Trajectory Design for $K = 2$

We first discuss the two segment case for an easy elaboration of the design concept. Here, \mathcal{D}_1 corresponds to the LOS segment and \mathcal{D}_2 corresponds to the NLOS segment.

An example search trajectory in the polar coordinate system is visualized in Fig. 4 for easy illustration, where the black curve represents the search trajectory and the dashed gray curves represent the contours of the cost function $F_1(\rho, \theta)$. Note that $f(g_u(\mathbf{x}), g_b(\mathbf{x})) = F_1(\rho, \theta)$ when $\mathbf{x}(\rho, \theta) \in \mathcal{D}_1$ in the LOS region (unshaded area), and $f(g_u(\mathbf{x}), g_b(\mathbf{x})) = F_2(\rho, \theta)$ when $\mathbf{x}(\rho, \theta) \in \mathcal{D}_2$ in the NLOS region (shaded area). The UAV search trajectory in the two propagation segment case can be described as follows.

1) *Search on the BS-user Axis:* Let the UAV start from the BS. It first moves towards the user until it finds two critical positions (if they exist) $\mathbf{x}_k^0 = \mathbf{x}(\rho_k^0, 0)$, $k = 1, 2$, which correspond to the points achieving the minimum cost over the BS-user axis in the LOS region and NLOS region, respectively. Specifically, the parameters ρ_k^0 are the solutions that minimize $F_k(\rho, 0)$ subject to $\mathbf{x}(\rho, 0) \in \mathcal{D}_k$, for $k = 1, 2$, in the two segment case.

For example, when the UAV is initially in the NLOS region, it can move up to the LOS-NLOS boundary; with that, it can solve for ρ_1^0 and ρ_2^0 to obtain the critical points \mathbf{x}_1^0 and \mathbf{x}_2^0 . On the other hand, when the UAV is initially in the LOS region, it can compute the critical position \mathbf{x}_1^0 in the LOS region, while \mathbf{x}_2^0 does not exist.

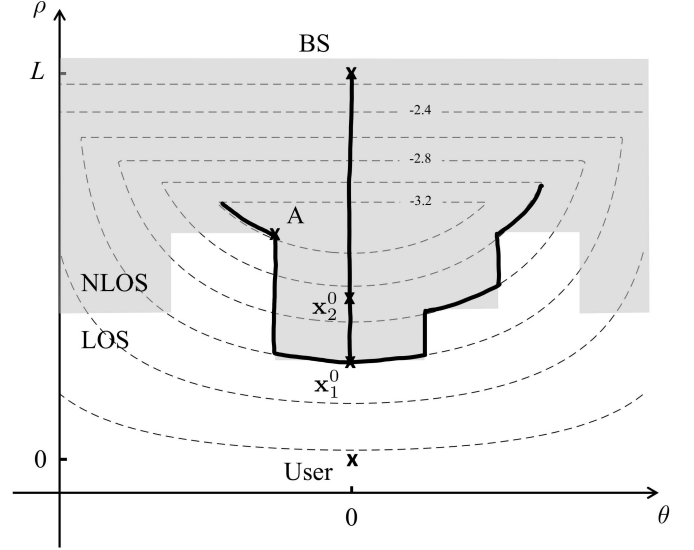


Figure 4. An example of UAV search trajectory under two propagation segment case. The dashed lines represent the contours of the cost function.

2) *Search on the Right Branch:* Starting from the critical position \mathbf{x}_1^0 , the UAV first moves to $\mathbf{x}(\rho_1^0, \delta/\rho_1^0)$, i.e., a position just on the right of \mathbf{x}_1^0 in Fig. 4, where δ is some step size. It then proceeds according to the following two phases, and at the same time, keeps track of the minimum cost value, denoted as F_{\min} , and the corresponding position, denoted as $\hat{\mathbf{x}}$, along the search trajectory:

- If the UAV is in the LOS region, it moves away from the user. Specifically, it moves from $\mathbf{x}(\rho, \theta)$ to $\mathbf{x}(\rho + \delta, \theta)$.
- If the UAV is in the NLOS region, it moves along the contour of $F_1(\rho, \theta)$. Specifically, the contour $F_1(\rho, \theta) = C$ satisfies³

$$\frac{\partial F_1(\rho, \theta)}{\partial \rho} d\rho + \frac{\partial F_1(\rho, \theta)}{\partial \theta} d\theta = 0.$$

It can be shown that (Lemma 4 in Appendix C), $\partial F_1(\rho, \theta)/\partial \theta \neq 0$ for $\theta \neq 0$. As a result from (7), we have

$$d\mathbf{x} = \mathbf{M}(\theta)\mathbf{u}d\rho + \rho \frac{d}{d\theta} \mathbf{M}(\theta)\mathbf{u} \left(-\frac{\partial F_1}{\partial \theta} \right)^{-1} \frac{\partial F_1}{\partial \rho} d\rho.$$

Thus, the UAV updates its position from \mathbf{x} to $\mathbf{x} + \Delta\mathbf{x}$, where

$$\Delta\mathbf{x} = \gamma \left[\mathbf{M}(\theta)\mathbf{u} + \rho \frac{d}{d\theta} \mathbf{M}(\theta)\mathbf{u} \left(-\frac{\partial F_1}{\partial \theta} \right)^{-1} \frac{\partial F_1}{\partial \rho} \right]$$

in which, $\gamma > 0$ is chosen such that $\|\Delta\mathbf{x}\| = \delta$. The constraint $\gamma > 0$ is to guarantee that the UAV keeps moving away from the user (see Fig. 4).

The search at this branch is completed whenever the UAV reaches a point $\mathbf{x}(\rho, \theta)$ such that either $\partial F_1(\rho, \theta)/\partial \rho \geq 0$ or $\rho \geq L \cos \theta$, where $L \triangleq \|\mathbf{x}_b - \mathbf{x}_u\|$. The justification of the two stopping criteria will become clear in Section IV-A.

³For mathematical completeness, the partial derivative is defined as $\frac{\partial f(x_0, y_0)}{\partial x} = \lim_{t \rightarrow 0} \frac{1}{t} [f(x_0 + t, y_0) - f(x_0, y_0)]$ throughout this paper.

Algorithm 1 Search Trajectory for Optimal UAV Position

Choose a step size $\delta > 0$.

- 1) **Search on the BS-user axis:** Find the critical points ρ_k^0 , $k = 1, 2, \dots, K$, defined in (14). Initialize $F_{\min} = F_1(\rho_1^0, 0)$ and $\hat{\mathbf{x}} = \mathbf{x}(\rho_1^0, 0)$, where $\mathbf{x}(\rho, \theta)$ is defined in (7). Initialize $k = 1$.
- 2) **Search on the right branch:** Set $\mathbf{x} \leftarrow \mathbf{x}(\rho_k^0, \delta/\rho_k^0)$.
- 3) For each iterate \mathbf{x} , compute $\rho = \|\mathbf{x} - \mathbf{x}_u\|$ and θ from (9).
 - a) **Search in the virtual LOS region:** If $\mathbf{x} \in \bigcup_{j=1}^k \mathcal{D}_j$, update

$$\mathbf{x} \leftarrow \mathbf{x}(\rho + \delta, \theta) \quad (12)$$

When $F_k(\rho + \delta, \theta) < F_{\min}$, then update the record $F_{\min} \leftarrow F_k(\rho + \delta, \theta)$ and $\hat{\mathbf{x}} \leftarrow \mathbf{x}(\rho + \delta, \theta)$.

- b) **Search in the virtual NLOS region:** If $\mathbf{x} \notin \bigcup_{j=1}^k \mathcal{D}_j$, update $\mathbf{x} \leftarrow \mathbf{x} + \Delta \mathbf{x}$, where

$$\Delta \mathbf{x} = \gamma \left[\mathbf{M}(\theta) \mathbf{u} + \rho \frac{d}{d\theta} \mathbf{M}(\theta) \mathbf{u} \left(-\frac{\partial F_k}{\partial \theta} \right)^{-1} \frac{\partial F_k}{\partial \rho} \right] \quad (13)$$

where $\gamma > 0$ is chosen such that $\|\Delta \mathbf{x}\| = \delta$.

Repeat this step until either (i) $\rho \geq L \cos \theta$ or (ii) $\partial F_k(\rho, \theta)/\partial \rho \geq 0$.

- 4) **Search on the left branch:** Set $\mathbf{x} \leftarrow \mathbf{x}(\rho_k^0, -\delta/\rho_k^0)$. Repeat Step 3).
- 5) Let $k \leftarrow k + 1$. Repeat from Step 2) until $k > K - 1$.
- 6) If $F_K(\rho_K^0, 0) < F_{\min}$, then $F_{\min} \leftarrow F_K(\rho_K^0, 0)$ and $\hat{\mathbf{x}} \leftarrow \mathbf{x}(\rho_K^0, 0)$.

3) *Search on the Left Branch:* Starting from the critical position \mathbf{x}_1^0 , the UAV moves to $\mathbf{x}(\rho_1^0, -\delta/\rho_1^0)$, i.e., a position just on the left of \mathbf{x}_1^0 in Fig. 4. It repeats the same process as in Section III-C2 until it meets the stopping criteria. When the search is completed, the minimum cost is found at F_{\min} with corresponding position recorded as $\hat{\mathbf{x}}$. Note that the optimal position $\hat{\mathbf{x}}$, for example, point A in Fig. 4, is *not* necessarily where the search terminates, because the cost f at $\mathbf{x}(\rho, \theta)$ may equal to $F_1(\rho, \theta)$ or $F_2(\rho, \theta)$ depending on whether \mathbf{x} is in LOS or NLOS.

We will show in Section IV-A that the above procedure finds the globally optimal UAV position at $\hat{\mathbf{x}}$ under some mild conditions on the cost function f .

D. Search Trajectory Design for Arbitrary K

In the case of more than two propagation segments, one can generate $K - 1$ search trajectories following a similar procedure in Section III-C, where each trajectory is computed by partitioning the whole area into two virtual propagation regions: *virtual LOS* region and *virtual NLOS* region. Specifically, for the k th search trajectory, the virtual LOS region is defined by grouping the first k propagation segments together $\tilde{\mathcal{D}}_k \triangleq \bigcup_{j=1}^k \mathcal{D}_j$, and correspondingly, the virtual NLOS region is defined as $\tilde{\mathcal{D}}_k^c \triangleq \mathbb{D} \setminus \tilde{\mathcal{D}}_k = \bigcup_{j=k+1}^K \mathcal{D}_j$. The whole algorithm can be summarized as follows.

- **Search on BS-user axis:** Let the UAV start from the BS. It first moves towards the user until it finds the $K - 1$ critical positions $\mathbf{x}_k^0 = \mathbf{x}(\rho_k^0, 0)$, $k = 1, K - 1$, each of which corresponds to a point achieving the minimum cost over the BS-user axis in a virtual LOS region. Specifically, the parameters ρ_k^0 are the solutions to

$$\underset{\rho \geq 0}{\text{minimize}} \quad F_k(\rho, 0) \quad (14)$$

$$\text{subject to} \quad \mathbf{x}(\rho, 0) \in \bigcup_{j=1}^k \mathcal{D}_j \quad (15)$$

for $k = 1, 2, \dots, K - 1$. In addition, ρ_K^0 is defined as the solution that minimizes (14) subject to $\mathbf{x}(\rho, 0) \in \mathcal{D}_K$. Similarly, it is sufficient for the UAV to move up to the boundary of the LOS region (propagation segment \mathcal{D}_1). With that, it can infer all the propagation segments over the BS-user axis from the nested segmented propagation property (3)–(4), and solve (14) for ρ_k^0 , $k = 1, 2, \dots, K$.

- **Search over $K - 1$ virtual LOS/NLOS partition scenarios:** In the k th search, $k = 1, 2, \dots, K - 1$, the UAV follows a similar procedure as that in Sections III-C2 and III-C3 for virtual LOS region $\tilde{\mathcal{D}}_k$ and virtual NLOS region $\tilde{\mathcal{D}}_k^c$.
- **Integration:** During the whole search, the UAV keeps track of the minimum achievable cost F_{\min} and the corresponding position $\hat{\mathbf{x}}$. When the algorithm terminates, $\hat{\mathbf{x}}$ gives the desired UAV position.

The entire search algorithm is summarized in Algorithm 1.

IV. GLOBAL OPTIMALITY AND LINEAR SEARCH LENGTH

To study the optimality of Algorithm 1, we focus on cost functions f that satisfy either one of the following conditions.

Condition 1. Assume that the cost function $f(x, y)$ in \mathcal{P} satisfies

$$x \frac{\partial^2 f(x, y)}{\partial x^2} + 2 \frac{\partial f(x, y)}{\partial x} \geq 0, \text{ and } y \frac{\partial^2 f(x, y)}{\partial y^2} + 2 \frac{\partial f(x, y)}{\partial y} \geq 0 \quad (16)$$

for every $x, y > 0$.

It can be easily verified that the outage probability minimization problem $\mathcal{P}1$ satisfies Condition 1. Note that Condition 1 does not require $f(x, y)$ to be convex.

Condition 2. Assume that the cost function $f(x, y)$ in \mathcal{P} can be written as $\max\{f_1(x), f_2(y)\}$, where $f_1(x)$ and $f_2(y)$ are decreasing functions.

It is also clear that the rate maximization problem $\mathcal{P}2$ satisfies Condition 2.

In addition, we focus on continuous-time algorithm trajectory $\mathbf{x}(t)$, which can be obtained from Algorithm 1 using infinitesimal step size $\delta = O(dt)$ at each infinitesimal time slot dt . Specifically, the search trajectory $\mathbf{x}(t)$ in Algorithm 1 can be described by piece-wise continuous dynamic systems, where one replaces δ by κdt in (12) and γ by $\kappa \gamma dt$ in (13), in which κ is a parameter that specifies the moving speed of the UAV. Accordingly, the continuous-time processes of the minimum cost $F_{\min}(t)$ and

the position track record $\hat{\mathbf{x}}(t)$ are given by $F_{\min}(t) = \min_{0 \leq \tau \leq t} f(g_u(\mathbf{x}(\tau), g_b(\mathbf{x}(\tau)))$ and $\hat{\mathbf{x}}(t) = \mathbf{x}(\hat{\tau})$, respectively, where $\hat{\tau} = \arg \min_{0 \leq \tau \leq t} f(g_u(\mathbf{x}(\tau), g_b(\mathbf{x}(\tau)))$.

A. Global Optimality

We first present the main optimality result as follows.

Theorem 1 (Global Optimality). *Suppose that the cost function f in \mathcal{P} satisfies either Condition 1 or Condition 2. Then, $\hat{\mathbf{x}}(t)$ in Algorithm 1 converges to the globally optimal solution to \mathcal{P} and $F_{\min}(t)$ converges to the minimum cost value.*

Theorem 1 establishes a powerful result that, the globally optimal UAV position is attainable, even though the terrain topology could be arbitrarily complex. As a practical implication, the result suggests that, even when the propagation gaps between buildings are small (leading to many “spines” in the irregular propagation segments as shown in Fig. 2(c)), one can always choose a small enough step size $\delta < \bar{\delta}(\epsilon)$ in Algorithm 1, such that the algorithm search trajectory will visit the neighborhood of the globally optimal UAV position with probability $1 - \epsilon$, close to 1.

Note that the globally optimality result does not require convexity or first order continuity of the objective function.

The optimality result can be derived using the polar coordinate system. From the definition of the k th fictitious segment cost function $F_k(\rho, \theta)$ in (10), problem \mathcal{P} can be equivalently written as

$$\mathcal{P}' : \quad \underset{\rho \geq 0, -\pi \leq \theta \leq \pi}{\text{minimize}} \quad F(\rho, \theta) \triangleq \sum_{k=1}^K F_k(\rho, \theta) \mathbb{I}\{(\rho, \theta) \in \mathcal{P}_k\}$$

where $\mathcal{P}_k \triangleq \{(\rho, \theta) : \mathbf{x}(\rho, \theta) \in \mathcal{D}_k\}$ is the k th propagation segment in the polar coordinate system. The optimal solution \mathbf{x}^* to \mathcal{P} can be obtained as $\mathbf{x}^* = \mathbf{x}(\rho^*, \theta^*)$, in which (ρ^*, θ^*) is the optimal solution to \mathcal{P}' .

The following intermediate results provide some intuitions to understand the optimality result in Theorem 1.

Proposition 2 (Bounded Search Region). *The optimal solution \mathbf{x}^* to \mathcal{P} can be obtained as $\mathbf{x}(\rho^*, \theta^*)$, where $(\rho^*, \theta^*) \in \mathcal{P}$ and*

$$\mathcal{P} = \left\{(\rho, \theta) : 0 \leq \rho \leq L \cos \theta, -\frac{\pi}{2} \leq \theta \leq \frac{\pi}{2}\right\} \quad (17)$$

in which, $L \triangleq \|\mathbf{x}_b - \mathbf{x}_u\|$ is the ground projected distance from the BS to the user.

Proof. Please refer to Appendix A. \square

Proposition 2 justifies the first stopping criterion $\rho \geq L \cos \theta$ in Step 3) of Algorithm 1. An intuitive explanation is that when the UAV moves outside the region \mathcal{P} in (17), one can always find a position in \mathcal{P} that has a equal (or smaller) distances, respectively, to the BS and to the user in the same (or less obstructed) propagation segment \mathcal{D}_k , leading to an equal (or lower) cost to achieve. Therefore, the optimal UAV position is contained in \mathcal{P} .

The following proposition justifies the second stopping criterion $\partial F_k(\rho, \theta)/\partial \rho \geq 0$.

Proposition 3 (Partial Optimality). *Suppose that the cost function f in \mathcal{P} satisfies either Condition 1 or Condition 2. Then, $F_k(\rho, \theta)$ admits a unique local minimizer $\rho_k^*(\theta)$ over $\rho \geq 0$ for every fixed θ , where $|\theta| < \pi/2$.*

Proof. Please refer to Appendix B. \square

Due to the fact that $F_k(\rho, \theta)$ has a unique local minimum for every θ , condition $\partial F_k(\rho, \theta)/\partial \rho \geq 0$ implies that $\rho \geq \rho_k^*(\theta)$. On the other hand, Step 3) of Algorithm 1 always increases ρ (to be formally justified in Lemma 10 in Appendix E). Therefore, it suffices to stop the search when the condition $\partial F_k(\rho, \theta)/\partial \rho \geq 0$ is met.

Leveraging the important results in Propositions 2 and 3, the proof of Theorem 1 is derived in Appendix C under the two segment case, $K = 2$. The result is then generalized to the case of arbitrary number of segments $K \geq 2$ in Appendix D.

B. Maximum Length of the Algorithm Trajectory

Here, we derive the worst-case trajectory length of Algorithm 1.

Theorem 2 (Maximum Trajectory Length). *The length of the search trajectory from Algorithm 1 is upper bounded by $(2.4K - 1.4)L$.*

Proof. Please refer to Appendix E. \square

Theorem 2 suggests that the algorithm must terminate in a finite number of steps given a positive step size $\delta > 0$. Surprisingly, the bound is linear in L and does not depend on the shapes of the propagation segments \mathcal{D}_k . As a benchmark, if one searches the optimal UAV position following the segment boundaries (a property from Proposition 1), the worst-case length of search will scale as $\mathcal{O}(L^2)$, depending on the shapes of the boundaries (see, for example, Fig. 2(c)).

V. NUMERICAL RESULTS

Consider a dense urban area with buildings ranging from 5–45 meter height as illustrated in Fig. 2 (a). The user is represented by a red circle and the BS locates at the top right corner denoted by a blue triangle. The height of the BS is 45 meters, and the UAV moves at 50 meter above the ground. As a result, there is always LOS propagation between the UAV and the BS. Consider two propagation scenarios depending on whether there is LOS propagation between the UAV and the user. Correspondingly, the parameters of the UAV-BS channel (1) are chosen as $(\alpha_0, \log_{10} \beta_0) = (2.2, -4)$ and the parameters of the UAV-user channel (2) are chosen as $(\alpha_1, \log_{10} \beta_1, \alpha_2, \log_{10} \beta_2) = (2.2, -4, 3.6, -2.4)$ according to some proper scenarios chosen from the WINNER II channel measurement report [26].

We evaluate the UAV positioning algorithm for the end-to-end capacity maximization problem $\mathcal{P}2$. The transmission powers are chosen as $P_b = 30$ dBm from the BS and $P_d = 36$ dBm from the UAV, and the noise power is -80 dBm. The corresponding power map and end-to-end capacity map

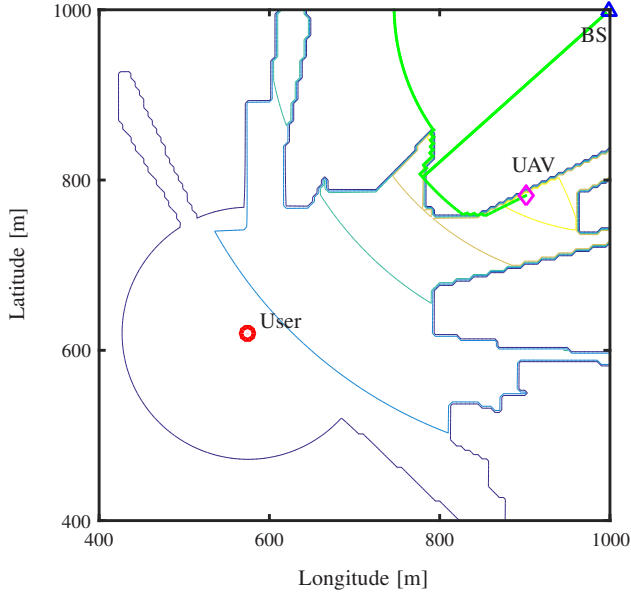


Figure 5. Search path (green lines) towards the optimal UAV position (purple diamond). The curves in other colors represent the contours of the end-to-end capacity (the constant objective value in (6) in $\mathcal{P}2$).

for every UAV position are illustrated in Fig. 2 (b) and (c). Due to the complex environment, finding the optimal UAV position for maximum end-to-end capacity is highly non-trivial as shown in Fig. 2 (c).

A. Demonstration of the UAV Search Path

In Fig. 5 the green curves show the search path for the optimal UAV position in solving maximum end-to-end capacity problem $\mathcal{P}2$. The two curve branches correspond to the UAV searches in Step 2) and Step 4) in Algorithm 1, respectively. The other curves in Fig. 5 represent the contour of equal end-to-end capacity. The optimal UAV position is found at the purple diamond.

B. Throughput Performance

We now evaluate the throughput performance with the UAV relay. Consider that a single user locates randomly and uniformly on the streets depicted in Fig. 2 (a). The transmission powers are chosen as $P_b = P_d = 33$ dBm for both the BS and the UAV, and the throughput is evaluated as the absolute value of (6). The proposed scheme places the UAV to the position obtained from Algorithm 1 under step size $\delta = 5$ meters. We also consider the following baselines for UAV positioning:

- **Probabilistic Algorithm** [16]: First, obtain an empirical LOS distribution $f_{\text{LOS}}(\varphi) = \mathbb{P}\{\text{LOS}, \varphi\}$ as a function of the elevation angle φ from the user to the UAV, by uniformly and randomly dropping 10,000 users on the streets in Fig. 2 (a) and randomly picking UAV locations within the target area. Second, given each user position \mathbf{x}_u , the UAV-user channel at UAV location \mathbf{x} is computed as [13], [16]

$$g_u(\mathbf{x}) = f_{\text{LOS}}(\varphi)\beta_1\|\mathbf{x} - \mathbf{x}_u\|^{-\alpha_1} + (1 - f_{\text{LOS}}(\varphi))\beta_2\|\mathbf{x} - \mathbf{x}_u\|^{-\alpha_2}. \quad (18)$$

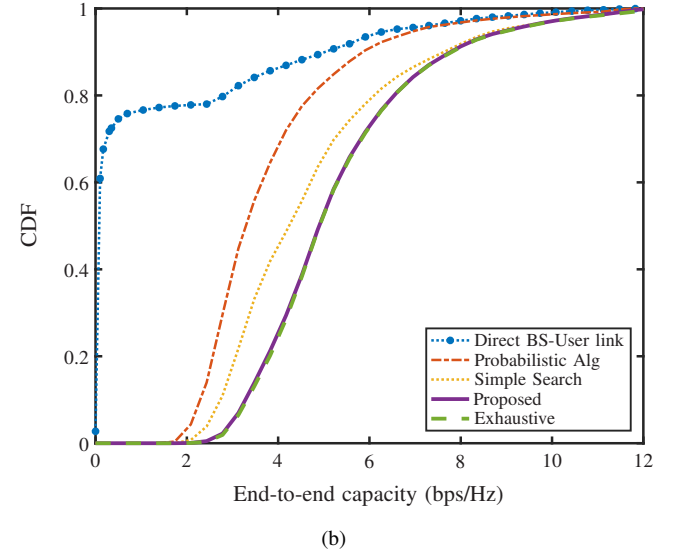
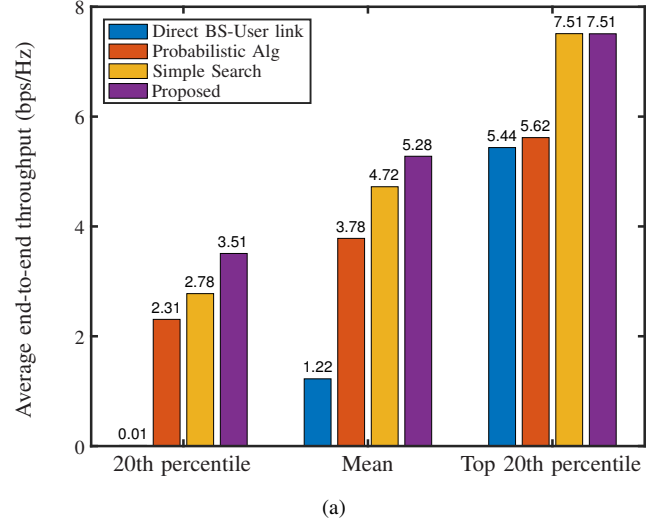


Figure 6. Comparison of the average end-to-end throughput over different schemes.

The optimal UAV position is then obtained by solving $\mathcal{P}2$ based on the function $g_u(\mathbf{x})$ in (18).

- **Simple Search:** Obtain the optimal UAV position by searching only on the BS-user axis (*i.e.*, to implement only Step 1) of Algorithm 1).
- **Exhaustive Search:** We perform exhaustive search over the entire search region on equally-spaced grids with $\delta = 5$ meter spacing. The grid point that maximizes the objective in $\mathcal{P}2$ is chosen as the UAV position. Note that such a scheme is prohibited in practice and hence it is for benchmarking only.

The performance on direct BS-user transmission (without UAV relaying) is evaluated using the segmented channel model (2) by replacing $d_u(\mathbf{x})$ by the BS-user distance and replacing $\mathbb{I}\{\mathbf{x} \in \mathcal{D}_k\}$ by the indicator of the BS-user link propagation segment.

Fig. 6 compares the average end-to-end throughput over 10,000 users in Fig. 2 (a). The cell edge users are recognized as those within the 20th percentile of the throughput under direct

BS-user transmission, and the cell center users are recognized as those in the top 20th percentile.⁴ First, the proposed scheme performs as well as the exhaustive search scheme as seen from the two overlapping cumulative distribution function (CDF) curves, which verify our theoretical results on optimality. Second, across all the three user categories, the proposed scheme with the optimal UAV placement achieves the highest throughput. In particular, it realizes more than 300% throughput gain on average over direct BS-user transmission, and achieves 50% gain for cell edge users over an probabilistic approach.

VI. CONCLUSION

This paper designed algorithms to search for the optimal UAV position for establishing the best wireless relay link between a BS and a user in a dense urban area. Global topological information, such as the location and the volume of the buildings, was not required. The desired UAV position, constrained at a fixed height above the ground, was defined as the minima of a general cost function. A nested segmented propagation model was proposed to model the propagation from the UAV to the ground user that is probably blocked by obstacles. A search algorithm was developed and shown to find the global optimal UAV position. In addition, the length of the search trajectory is upper bounded by a linear function of the BS-user distance. Significant throughput gains are found when compared to other UAV positioning approaches or direct BS-user transmissions.

APPENDIX A

PROOF OF PROPOSITION 2

We establish the following lemma, which implies that a smaller cost value can be achieved in a less obstructed propagation segment.

Lemma 1 (Less Obstructed Segmented is Preferred). *Given ρ and θ , the following holds*

$$F_k(\rho, \theta) < F_{k+1}(\rho, \theta) \quad (19)$$

for $k = 1, 2, \dots, K - 1$.

Proof. From the nested segmented propagation property (3) – (4) and the definition of $g_u^{(k)}(\mathbf{x})$ in (11), we have $g_u^{(k)}(\mathbf{x}(\rho, \theta)) > g_u^{(k+1)}(\mathbf{x}(\rho, \theta))$ for all $\mathbf{x}(\rho, \theta)$. Since $f(g_u, g_b)$ is a decreasing function in g_u , we have the inequality (19) from the definition of $F_k(\rho, \theta)$ in (10). \square

The result of Proposition 2 can be proven by contradiction as follows.

First, suppose that solution $\mathbf{x}(\rho', \theta')$ satisfies $\frac{\pi}{2} < |\theta'| < \pi$. Then, we must have $F_1(\rho', \theta') \leq F(\rho', \theta')$ by Lemma 1 as \mathcal{P}_k are mutually exclusive. Since there is LOS propagation when the UAV is on top of the outdoor user, i.e., $(0, 0) \in \mathcal{P}_1$, we have $F(0, 0) = F_1(0, 0) < F_1(\rho', \theta') \leq F(\rho', \theta')$, where, by moving from $(0, 0)$ to (ρ', θ') , the UAV position (ρ', θ') has longer distances to both the user and the BS. Thus, by

contradiction, $\mathbf{x}(\rho', \theta')$ cannot be the optimal solution to \mathcal{P} , i.e., we must have $|\theta'| \leq \frac{\pi}{2}$.

Second, suppose that the optimal solution $\mathbf{x}(\rho', \theta')$ satisfies $\rho' > L \cos \theta'$. Consider a different solution $\mathbf{x}(\rho'', \theta')$, where $\rho'' = L \cos \theta' - (\rho' - L \cos \theta')$. From geometry, one can easily show that the UAV-BS distance $d_b(\mathbf{x}(\rho', \theta')) = d_b(\mathbf{x}(\rho'', \theta'))$ and the UAV-user distance $d_u(\mathbf{x}(\rho'', \theta')) < d_u(\mathbf{x}(\rho', \theta'))$. Suppose that $(\rho', \theta') \in \mathcal{P}_k$ and $(\rho'', \theta') \in \mathcal{P}_j$. From the nested segmented property (3) – (4), we must have $j \leq k$. From Lemma 1, we have

$$F(\rho'', \theta') = F_j(\rho'', \theta') < F_k(\rho'', \theta') < F_k(\rho', \theta') = F(\rho', \theta')$$

which contradicts to the hypothesis that (ρ', θ') minimizes the objective function $F(\rho, \theta)$. This confirms that the optimal solution must satisfies $0 \leq \rho \leq L \cos \theta$. \blacksquare

APPENDIX B

PROOF OF PROPOSITION 3

A. Proof under Condition I

We first analyze the property of the composite function $f((g_u \circ d_u)(\mathbf{z}), (g_b \circ d_b)(\mathbf{z}))$.

Lemma 2. *Let $g_i(d_i) = \beta_i d_i^{-\alpha_i}$, $i = 1, 2$, and $\alpha > 1$. Let $d_i(\mathbf{z})$, $i = 1, 2$, be convex functions in \mathbf{z} . Suppose that $f(x, y)$ satisfies Condition 1. Then, the composite function $f((g_1 \circ d_1)(\mathbf{z}), (g_2 \circ d_2)(\mathbf{z}))$ is strictly convex in \mathbf{z} .*

Proof. Since $\partial f / \partial x < 0$ and $\partial f / \partial y < 0$, the first order partial derivative of $f(g_1 \circ d_1, g_2 \circ d_2)$ is given by

$$\frac{\partial f}{\partial d_i} = \frac{\partial f}{\partial g_i} \frac{\partial g_i}{\partial d_i} = \frac{\partial f}{\partial g_i} (-\alpha_i \beta_i) d_i^{-\alpha_i-1} > 0$$

for $i = 1, 2$, and the second order partial derivative is given by

$$\begin{aligned} \frac{\partial^2 f}{\partial d_i^2} &= \frac{\partial^2 f}{\partial g_i^2} \frac{\partial g_i}{\partial d_i} (-\alpha_i \beta_i) d_i^{-\alpha_i-1} + (-\alpha_i \beta_i) \frac{\partial f}{\partial g_i} \frac{\partial}{\partial d_i} d_i^{-\alpha_i-1} \\ &= \alpha_i^2 \beta_i d_i^{-\alpha_i-2} \left(\beta_i d_i^{-\alpha_i} \frac{\partial^2 f}{\partial g_i^2} + \frac{\alpha_i + 1}{\alpha_i} \frac{\partial f}{\partial g_i} \right) \\ &> \alpha_i^2 \beta_i d_i^{-\alpha_i-2} \left(g_i \frac{\partial^2 f}{\partial g_i^2} + 2 \frac{\partial f}{\partial g_i} \right) \\ &\geq 0 \end{aligned}$$

for $i = 1, 2$, where the first inequality is due to the fact that $\alpha_i > 1$ and $\frac{\partial f}{\partial g_i} < 0$.

Define an operator $\nabla \triangleq [\frac{\partial}{\partial z_1} \frac{\partial}{\partial z_2} \dots \frac{\partial}{\partial z_m}]^T$, where z_i is the i th entry of a vector variable \mathbf{z} . From $\nabla f = \frac{\partial f}{\partial d_1} \nabla d_1 + \frac{\partial f}{\partial d_2} \nabla d_2$, the Hessian matrix of f is given by

$$\begin{aligned} \nabla^2 f &= \frac{\partial^2 f}{\partial d_1^2} \nabla d_1 \nabla d_1^T + \frac{\partial f}{\partial d_1} \nabla^2 d_1 \\ &\quad + \frac{\partial^2 f}{\partial d_2^2} \nabla d_2 \nabla d_2^T + \frac{\partial f}{\partial d_2} \nabla^2 d_2 \succeq \mathbf{0} \end{aligned}$$

since $\nabla^2 d_i(\mathbf{z}) \succeq \mathbf{0}$ due to the convexity of $d_i(\mathbf{z})$. Therefore, f is strictly convex in \mathbf{z} (as $d_i(\mathbf{z})$ are strictly convex). \square

⁴We found from our experiment that around 22% users have LOS propagation on the BS-user link.

From the polar representation of the UAV-user and UAV-BS distances

$$d_b(\mathbf{x}(\rho, \theta)) = \sqrt{\rho^2 + L^2 - 2\rho L \cos \theta + (H_d - H_b)^2} \quad (20)$$

$$d_u(\mathbf{x}(\rho, \theta)) = \sqrt{\rho^2 + (H_d - H_u)^2} \quad (21)$$

one can show that $d_b(\mathbf{x}(\rho, \theta))$ and $d_u(\mathbf{x}(\rho, \theta))$ are strictly convex in ρ .

Then, using Lemma 2 and the definition of $F_k(\rho, \theta)$ in (10), we can conclude that $F_k(\rho, \theta)$ is strictly convex in ρ , and therefore, $F_k(\rho, \theta)$ admits a unique local minima $\rho_k^*(\theta)$ in the bounded interval $\rho \in [0, L \cos \theta]$.

B. Proof under Condition II

Consider $F_k(\rho, \theta) = \max\{f_1(g_u^{(k)}(\mathbf{x}(\rho, \theta))), f_2(g_b(\mathbf{x}(\rho, \theta)))\}$. From (20) – (21), to increase ρ , we must have d_u increase and d_b decrease, and as a result, f_1 decreases and f_2 increases monotonically in $\rho \in [0, L \cos \theta]$. Therefore, there exists a unique local minimizer $\rho_k^*(\theta)$ in the closed interval $[0, L \cos \theta]$. ■

APPENDIX C

PROOF OF THEOREM 1 UNDER $K = 2$ CASE

From the bounded search region result established in Appendix A (see Proposition 2), we can focus on $-\frac{\pi}{2} < \theta < \frac{\pi}{2}$. As a result, the algorithm trajectory $\mathbf{x}(t)$ can be written as $(\rho(t), \theta(t))$ via the inverse of the mapping $\mathbf{x}(\rho(t), \theta(t))$ from (7). In addition, defining the process $(\hat{\rho}(t), \hat{\theta}(t))$ from $\hat{\mathbf{x}}(t)$, the convergence of the process $\hat{\mathbf{x}}(t)$ corresponds to the convergence of $(\hat{\rho}(t), \hat{\theta}(t))$. With these notations, we will work on the polar coordinate system for the optimality proof.

We first focus on the subproblem

$$\mathcal{P}'_+ : \underset{\rho \geq 0, 0 \leq \theta \leq \frac{\pi}{2}}{\text{minimize}} \quad F(\rho, \theta)$$

which corresponds to the search on the right branch illustrated in Fig. 4.

To show the optimality in \mathcal{P}'_+ , we note that when the algorithm terminates at $t = T$, $F_{\min}(T)$ satisfy

$$F_{\min}(T) \leq \underset{0 \leq \rho \leq L}{\text{minimize}} \quad F(\rho, 0) \quad (22)$$

$$= \underset{\rho \geq 0}{\text{minimize}} \quad F(\rho, 0) \quad (23)$$

$$\leq \underset{\rho \geq 0}{\text{minimize}} \quad F_2(\rho, 0) \quad (24)$$

$$\leq \underset{\rho \geq 0, (\rho, \theta) \in \mathcal{P}_2}{\text{minimize}} \quad F_2(\rho, \theta) \quad (25)$$

where inequality (22) is due to Step 1) and 6) in Algorithm 1 and the fact that $F_{\min}(t)$ is a non-increasing process. Equality (23) is due Proposition 2, inequality (24) is due to Lemma 1 in Appendix A, and inequality (25) is from Lemma 4 to be developed later.

We then state the following lemma, for which the proof will be established later.

Lemma 3 (Local optimality). *Suppose that the cost function f in \mathcal{P} satisfies either condition I or condition II. Then, the continuous trajectory $(\rho(t), \theta(t))$ passes through (ρ^*, θ^*) before it completes Step 3) in Algorithm 1 at $t = T_3$, i.e., there*

exists $t^ \leq T_3$, such that $\rho(t^*) = \rho^*$ and $\theta(t^*) = \theta^*$, where (ρ^*, θ^*) is the optimal solution to the following problem*

$$\underset{\rho \geq 0, (\rho, \theta) \in \mathcal{P}_1^+}{\text{minimize}} \quad F_1(\rho, \theta) \quad (26)$$

where $\mathcal{P}_1^+ = \{(\rho, \theta) : 0 \leq \theta \leq \frac{\pi}{2}, (\rho, \theta) \in \mathcal{P}_1\}$.

Using Lemma 3, the record $F_{\min}(T_3)$ satisfies

$$F_{\min}(T_3) \leq \underset{\rho \geq 0, (\rho, \theta) \in \mathcal{P}_1^+}{\text{minimize}} \quad F_1(\rho, \theta). \quad (27)$$

Finally, similar arguments from Lemma 3 can apply to Step 4) which yields

$$F_{\min}(T_4) \leq \underset{\rho \geq 0, (\rho, \theta) \in \mathcal{P}_1^-}{\text{minimize}} \quad F_1(\rho, \theta) \quad (28)$$

where $\mathcal{P}_1^- = \{(\rho, \theta) : -\frac{\pi}{2} \leq \theta \leq 0, (\rho, \theta) \in \mathcal{P}_1\}$ and $T_4 > T_3$ is the time when the algorithm completes Step 4).

Since $F_{\min}(t)$ is a non-increasing process, to summarize from (25), (27), and (28), $F_{\min}(T)$ gives the minimum value over subset \mathcal{P}_2 , \mathcal{P}_1^+ , and \mathcal{P}_1^- , and hence achieves the minimum value of \mathcal{P}' , i.e., the minimum value of \mathcal{P} . As a result, $(\hat{\rho}(t), \hat{\theta}(t))$ converges to the optimal solution to \mathcal{P}' before the entire algorithm terminates at $t = T$, which implies that $\hat{\mathbf{x}}(t)$ converges to the optimal solution to \mathcal{P} . ■

The remaining part of this section is to prove Lemma 3.

A. General Strategy to Prove Lemma 3

Before developing the technical details, the structure of the proof is sketched as follows.

- We first show that the algorithm trajectory $(\rho(t), \theta(t))$ in the loop of Step 3) can only stop at $\theta(T) \geq \theta^*$, where T is a finite stopping time (Lemma 7). Therefore, as the algorithm trajectory from Step 3) is continuous, we must have $\theta(t) = \theta^*$ for some $t \leq T$.
- We then argue that when the trajectory reaches $\theta(t) = \theta^*$ for some $t \leq T$, it must hold that $(\rho(t), \theta(t)) \in \mathcal{P}_1^+$ and $\rho(t) \leq \rho^*$ (Lemma 8).
- As a result, by Step 3a) in Algorithm 1, $(\rho(t), \theta(t))$ must then reach (ρ^*, θ^*) by increasing $\rho(t)$ until $\rho(t) = \rho^*$.

Therefore, the minimum objective value $F_{\min} \leftarrow F_1(\rho^*, \theta^*)$ as well as the optimal solution (ρ^*, θ^*) to the subproblem (26) are discovered and recorded in processes $F_{\min}(t)$ and $(\rho(t), \theta(t))$.

B. Preliminary Results

We need the following preliminary results to develop Lemmas 7 and 8.

First, the following property reduces the search space.

Lemma 4. *It holds that $\partial F_k(\rho, \theta) / \partial |\theta| > 0$ for all k and $\theta \neq 0$. In addition, for any $\theta' \geq 0$, the following property holds*

$$\min_{\rho \geq 0} F_k(\rho, \theta') \leq \min_{j \geq k} \min_{\rho \geq 0, \theta' < \theta \leq \frac{\pi}{2}} F_j(\rho, \theta) \quad (29)$$

for $1 \leq k \leq K$. Similarly, for any $\theta' < 0$,

$$\min_{\rho \geq 0} F_k(\rho, \theta') \leq \min_{j \geq k} \min_{\rho \geq 0, -\frac{\pi}{2} \leq \theta < \theta'} F_j(\rho, \theta) \quad (30)$$

Proof. We first note that $\frac{\partial}{\partial|\theta|}F_k(\rho, \theta) > 0$ for all $k = 1, 2, \dots, K$, because increasing $|\theta|$ will increase the UAV-BS distance d_b while the UAV-user distance $d_u = \rho$ is not affected, and hence $g_b(\mathbf{x}(\rho, \theta))$ is decreased. As the cost function $f(x, y)$ is increasing with x and y , respectively, due to conditions I or II, the cost $F_k(\rho, \theta)$ increases as $|\theta|$ increases.

Consider that $\theta' \geq 0$. For every $0 \leq \rho \leq L$, $\theta \geq \theta'$, and $j \geq k$, we must have

$$F_k(\rho, \theta') \leq F_j(\rho, \theta') \leq F_j(\rho, \theta).$$

As a result, $\min_{\rho \geq 0} F_k(\rho, \theta') \leq \min_{\rho \geq 0} F_j(\rho, \theta)$ for every $\theta > \theta'$. Hence the result (29) is confirmed.

The case of (30) can be shown in a similar way. \square

As a key property of Algorithm 1, the following lemma shows that every cost $F_1(\rho(t), \theta(t))$ along the algorithm trajectory $(\rho(t), \theta(t))$ is achievable as it were in the LOS region. Specifically, even when the actual cost $F(\rho(t), \theta(t)) = F_2(\rho(t), \theta(t)) > F_1(\rho(t), \theta(t))$, there exists a $0 \leq \tau < t$, such that $F(\rho(\tau), \theta(\tau)) = F_1(\rho(t), \theta(t))$.

Lemma 5. *For every point on the algorithm trajectory $(\rho(t), \theta(t))$, $0 \leq t \leq T$, there exists $0 \leq \tau \leq t$, such that $(\rho(\tau), \theta(\tau)) \in \mathcal{P}_1$ and*

$$F(\rho(\tau), \theta(\tau)) = F_1(\rho(\tau), \theta(\tau)) = F_1(\rho(t), \theta(t)).$$

Proof. If $(\rho(t), \theta(t)) \in \mathcal{P}_1$, we have $F(\rho(t), \theta(t)) = F_1(\rho(t), \theta(t))$ and $\tau = t$. If $(\rho(t), \theta(t)) \in \mathcal{P}_2$, then the algorithm is in the loop of Step 3b), where it follows the trajectory on the contour $F_1(\rho(t), \theta(t)) = C$. To trace backward, there must be a $0 \leq \tau < t$, such that $F_1(\rho(\tau), \theta(\tau)) = F_1(\rho(t), \theta(t))$ and $(\rho(\tau), \theta(\tau)) \in \mathcal{P}_1$. Note that the initial point $(\rho_1^0, 0)$ from Step 1) is in the LOS region \mathcal{P}_1 from the definition (7). \square

Finally, the following property show that $\partial F_1(\rho, \theta(t))/\partial \rho \leq 0$ until the algorithm terminates.

Lemma 6. *Let $\rho_1^*(\theta)$ minimize $F_1(\rho, \theta)$ over all $\rho \geq 0$ with θ fixed. Then, the algorithm trajectory $(\rho(t), \theta(t))$ satisfies $\rho(t) \leq \rho_1^*(\theta(t))$ and $\partial F_1(\rho(t), \theta(t))/\partial \rho \leq 0$ for all t before the iteration completes Step 3). Moreover, $\partial F_1(\rho, \theta(t))/\partial \rho \leq 0$ for all $0 \leq \rho \leq \rho(t)$. The same result holds for the search trajectory in Step 4).*

Proof. First, from the definition of ρ_1^0 in (14) and the nested segmented propagation property (3) – (4), we have $\rho_1^0 \leq \rho_1^*(0)$. This is because, we have $\mathbf{x}(\rho_1^0, 0) \in \mathcal{D}_1$ from (14), and hence, all the points $(\rho, 0)$, $0 \leq \rho \leq \rho_1^0$, are in the LOS region. As a result, if $\rho_1^0 > \rho_1^*(0)$, then $(\rho_1^*(0), 0)$ is also in the LOS region (satisfying the constraint (15)), which implies that $\rho_1^*(0)$ minimizes (14), yielding a contradiction. Therefore, from Step 1), we have the initial point $(\rho(0), \theta(0))$ satisfying $\theta(0) = 0$ and $\rho(0) = \rho_1^0 \leq \rho_1^*(0) = \rho_1^*(\theta(0))$.

Second, as the local minimizer $\rho_1^*(\theta)$ is unique from Proposition 3, we must have $\partial F_1(\rho, \theta)/\partial \rho < 0$ for $\rho < \rho_1^*(\theta)$ and $\partial F_1(\rho, \theta)/\partial \rho > 0$ for $\rho > \rho_1^*(\theta)$. (Note that there is no saddle point either, due to the strict convexity under Condition 1 and monotonicity of f_1 and f_2 under Condition 2.) Once

$\partial F_1(\rho(t), \theta(t))/\partial \rho \geq 0$, Step 3) is completed. As a result, it holds that $\rho(t) \leq \rho_1^*(\theta(t))$. \square

C. Proof of Lemma 3

We now prove the following results.

Lemma 7. *The algorithm trajectory in Step 3) $(\rho(t), \theta(t))$ can only stop at $\theta(T_3) = \theta' \geq \theta^*$ where (ρ^*, θ^*) is the optimal solution to (26).*

Proof. The result can be proven by contradiction. Suppose that Step 3) stops at $(\rho(T_3), \theta(T_3))$ where $\rho(T_3) = \rho'$ and $\theta(T_3) = \theta' < \theta^*$. As Step 3) is completed, either one of the stopping criteria should have been triggered.

First, suppose that the condition $\partial F_1(\rho', \theta')/\partial \rho \geq 0$ was triggered. From Lemma 5, there exists $\tau \leq T_3$, such that $F_1(\rho(\tau), \theta(\tau)) = F_1(\rho', \theta')$ and $(\rho(\tau), \theta(\tau)) \in \mathcal{P}_1^+$. From Lemma 6 and Proposition 3, (ρ', θ') minimizes $F_1(\rho, \theta')$ over $\rho \geq 0$. As a result,

$$\begin{aligned} F_1(\rho(\tau), \theta(\tau)) &= F_1(\rho', \theta') \\ &= \underset{\rho \geq 0}{\text{minimize}} F_1(\rho, \theta') \\ &\leq \min_{j \geq 1} \underset{\rho \geq 0, \theta' < \theta \leq \frac{\pi}{2}}{\text{minimize}} F_j(\rho, \theta) \end{aligned} \quad (31)$$

$$\leq \underset{\rho \geq 0, \theta' < \theta \leq \frac{\pi}{2}}{\text{minimize}} F_1(\rho, \theta) \quad (32)$$

$$\begin{aligned} &\leq \underset{\rho \geq 0, \theta' < \theta \leq \frac{\pi}{2}, (\rho, \theta) \in \mathcal{P}_1^+}{\text{minimize}} F_1(\rho, \theta) \\ &= F_1(\rho^*, \theta^*) \end{aligned}$$

where inequality (31) is from Lemma 4, inequality (32) is from Lemma 1, and the last equality is by the hypothesis that $\theta^* > \theta'$. However, this violates the assumption that (ρ^*, θ^*) is the solution to (26), whereas, $(\rho(\tau), \theta(\tau)) \in \mathcal{P}_1^+$ yields a lower cost. By contradiction, the stopping criterion $\partial F_1(\rho', \theta')/\partial \rho \geq 0$ is not satisfied.

Second, suppose that the condition $\rho(T_3) = \rho' \geq L \cos \theta'$ is triggered. From Proposition 2 and the hypothesis that $\theta(T_3) = \theta' < \theta^*$, we have

$$\rho' \geq L \cos \theta' > L \cos \theta^* \geq \rho^*.$$

From Lemma 6, $\rho_1^*(\theta') > \rho'$ and $\partial F_1(\rho, \theta')/\partial \rho < 0$ for $\rho' \geq \rho \geq \rho^*$. As a result,

$$F_1(\rho', \theta') < F_1(\rho^*, \theta') < F_1(\rho^*, \theta^*) \quad (33)$$

where the second inequality is from Lemma 4.

From Lemma 5, there exists $\tau \leq T_3$, such that $(\rho(\tau), \theta(\tau)) \in \mathcal{P}_1^+$ and $F_1(\rho(\tau), \theta(\tau)) = F_1(\rho', \theta') < F_1(\rho^*, \theta^*)$, which contradicts to the hypothesis that (ρ^*, θ^*) is the solution to (26). Therefore, the stopping criterion $\rho(T_3) = \rho' \geq L \cos \theta'$ is not satisfied either.

To conclude, since neither of the stopping criteria is triggered, by contradiction, the algorithm can only stop at $\theta(T_3) \geq \theta^*$. \square

Note that the trajectory from Step 3) is continuous. Suppose that the trajectory reaches θ^* at time t_1 , i.e., $\theta(t_1) = \theta^*$ and $\theta(t) \leq \theta^*$ for all $t \leq t_1$. It holds that $(\rho(t_1), \theta(t_1)) \in \mathcal{P}_1^+$ as stated in the following lemma.

Lemma 8. *The algorithm trajectory satisfies $(\rho(t_1), \theta(t_1)) \in \mathcal{P}_1^+$, where $t_1 \geq 0$ satisfies $\theta(t_1) = \theta^*$ and $\theta(t) \leq \theta^*$ for $t < t_1$.*

Proof. We note that $\rho(t_1) \leq \rho^*$. This is because if $\rho(t_1) > \rho^*$, we must have $F_1(\rho(t_1), \theta^*) < F_1(\rho^*, \theta^*)$, since $\partial F_1(\rho, \theta^*)/\partial \rho < 0$ for all $\rho(t_1) > \rho > \rho^*$ as from Lemma 6. As a result of Lemma 5, there exists $\tau \leq t_1$, such that $F_1(\rho(\tau), \theta(\tau)) = F_1(\rho(t_1), \theta^*) < F_1(\rho^*, \theta^*)$ and $(\rho(\tau), \theta(\tau)) \in \mathcal{P}_1^+$, which contradicts to the assumption that (ρ^*, θ^*) is the solution to (26).

As $(\rho^*, \theta^*) \in \mathcal{P}_1^+$, from the nested segmented propagation property (3) – (4), we can conclude that $(\rho(t_1), \theta(t_1)) \in \mathcal{P}_1^+$. \square

Since $(\rho(t_1), \theta(t_1)) \in \mathcal{P}_1^+$, $\rho(t)$ will increase to ρ^* following Step 3a) in Algorithm 1. This completes the proof that the algorithm trajectory passes through $(\rho(t_2), \theta(t_2)) = (\rho^*, \theta^*)$ at time t_2 , where $t_1 \leq t_2 \leq T_3$.

APPENDIX D

PROOF OF THEOREM 1 UNDER A GENERAL NUMBER OF K

A. The Main Proof

We first establish the following result.

Lemma 9 (Local Optimality after k Loops). *After the k th loop of Steps 2) – 4) in Algorithm 1 is completed at time $t = T_k$, the following holds,*

$$F_{\min}(T_k) \leq \underset{\theta \geq 0, (\rho, \theta) \in \mathcal{P}_k}{\text{minimize}} F_k(\rho, \theta) \quad (34)$$

for all $k = 1, 2, \dots, K - 1$. Moreover, (34) holds for $k = K$ when the entire algorithm terminates.

Theorem 1 is a direct result from Lemma 9, since (34) holds for $k = 1, 2, \dots, K$ and $F_{\min}(t)$ is non-increasing, which implies that $F_{\min}(T_K)$ is the global minimum value of \mathcal{P}' and $(\hat{\rho}(T_K), \hat{\theta}(T_K))$ is the globally optimal solution to \mathcal{P}' .

B. Proof of Lemma 9

For the k th search trajectory from Steps 2) – 4) in Algorithm 1 in the case $K > 2$, the iteration is equivalent to that in the two segment case, $K = 2$. Specifically, the virtual propagation segment partition $(\bar{\mathcal{D}}_k, \bar{\mathcal{D}}_k^c)$ in the k th outer loop for the case $K > 2$ corresponds to the LOS-NLOS partition $(\mathcal{D}_1, \mathcal{D}_2)$ for the $K = 2$ case. Moreover, the function F_k in the k th outer loop in for the case $K > 2$ corresponds to the function F_1 for the $K = 2$ case. Hence, using Lemma 3, Steps 2) – 4) equivalently solve

$$\mathcal{P}'_k : \underset{\theta \geq 0, (\rho, \theta) \in \tilde{\mathcal{P}}_k}{\text{minimize}} F_k(\rho, \theta) \quad (35)$$

where $\tilde{\mathcal{P}}_k \triangleq \bigcup_{j=1}^k \mathcal{P}_j$.

Denote the optimal solution to \mathcal{P}'_k as $(\hat{\rho}^{(k)}, \hat{\theta}^{(k)})$. The remaining part of the proof proceeds using induction.

First of all, we know that for $k = 1$, inequality (34) is true due to Lemma 3, since $\tilde{\mathcal{P}}_1 = \mathcal{P}_1$.

Second, suppose that inequality (34) is true for $i = 1, 2, \dots, k - 1$, where $1 < k \leq K - 1$. The argument can be divided into two cases:

- 1) If $(\hat{\rho}^{(k)}, \hat{\theta}^{(k)}) \in \mathcal{P}_k$, then (34) is true because $\mathcal{P}_k \subseteq \tilde{\mathcal{P}}_k$.
- 2) If $(\hat{\rho}^{(k)}, \hat{\theta}^{(k)}) \notin \mathcal{P}_k$, then it holds that $(\hat{\rho}^{(k)}, \hat{\theta}^{(k)}) \in \tilde{\mathcal{P}}_k \setminus \mathcal{P}_k = \bigcup_{i < k} \mathcal{P}_i$. Without loss of generality (w.l.o.g.), assume that $(\hat{\rho}^{(k)}, \hat{\theta}^{(k)}) \in \mathcal{P}_j$ for some $j \leq k - 1$. We thus have

$$\underset{\theta \geq 0, (\rho, \theta) \in \tilde{\mathcal{P}}_k}{\text{minimize}} F_k(\rho, \theta) = F_k(\hat{\rho}^{(k)}, \hat{\theta}^{(k)}) \quad (36)$$

$$\geq F_j(\hat{\rho}^{(k)}, \hat{\theta}^{(k)}) \quad (37)$$

$$\geq \underset{\theta \geq 0, (\rho, \theta) \in \tilde{\mathcal{P}}_j}{\text{minimize}} F_j(\rho, \theta) \quad (38)$$

$$\geq F_{\min}(T_j) \quad (39)$$

$$\geq F_{\min}(T_k) \quad (40)$$

where inequality (37) is from Lemma 1 in Appendix A, inequality (38) is due to assumption $(\hat{\rho}^{(k)}, \hat{\theta}^{(k)}) \in \mathcal{P}_j \subseteq \tilde{\mathcal{P}}_j$, and inequality (40) is due to $T_j \leq T_k$ for $j < k$ and $F_{\min}(t)$ is a non-increasing process. This shows that inequality (34) is also true for k .

Therefore, by induction, inequality (34) is true for all $k = 1, 2, \dots, K - 1$.

Finally, the last step in Algorithm 1 yields

$$\begin{aligned} F_{\min} &\leq F_K(\rho_K^*(0), 0) \\ &\leq \underset{\rho \geq 0, 0 < \theta \leq \frac{\pi}{2}}{\text{minimize}} F_K(\rho, \theta) \\ &\leq \underset{\theta \geq 0, (\rho, \theta) \in \mathcal{P}_K}{\text{minimize}} F_K(\rho, \theta) \end{aligned} \quad (41)$$

where inequality (41) is from Lemma 4.

As a result from the above three paragraphs, (34) holds for all $k = 1, 2, \dots, K$. \blacksquare

APPENDIX E

PROOF OF THEOREM 2

An important property of Algorithm 1 is that the segment of search trajectory in Step 3) does not “turn back”, and so does that in Step 4).

Lemma 10 (Monotonicity). *Step 3) in Algorithm 1 strictly and monotonically increases $\rho(t)$, and it also monotonically increases $|\theta(t)|$. Similar property holds in Step 4).*

Proof. In Step 3a), $\rho(t)$ strictly and monotonically increases, while $\theta(t)$ keeps unchanged. In Step 3b), we have (omitting the higher order term)

$$\begin{aligned} \rho + \Delta\rho &= \|\mathbf{x} + \Delta\mathbf{x} - \mathbf{x}_u\| \\ &= \sqrt{\|\mathbf{x} - \mathbf{x}_u\|^2 + 2(\mathbf{x} - \mathbf{x}_u)^T \Delta\mathbf{x} + \|\Delta\mathbf{x}\|^2} \\ &= \rho \left(1 + \frac{1}{\rho^2} (\mathbf{x} - \mathbf{x}_u)^T \Delta\mathbf{x} + o(\|\mathbf{x}\|) \right) \end{aligned}$$

and since $(\mathbf{x} - \mathbf{x}_u)/\rho = \mathbf{M}(\theta)\mathbf{u}$ from (7), we have

$$\begin{aligned} \Delta\rho &= \mathbf{u}^T \mathbf{M}(\theta)^T \Delta\mathbf{x} \\ &= \mathbf{u}^T \mathbf{M}(\theta)^T \mathbf{M}(\theta) \mathbf{u} \gamma \\ &\quad + \gamma \rho \mathbf{u}^T \mathbf{M}(\theta)^T \frac{d}{d\theta} \mathbf{M}(\theta) \mathbf{u} \left(-\frac{\partial F_k}{\partial \theta} \right)^{-1} \frac{\partial F_k}{\partial \rho} \end{aligned}$$

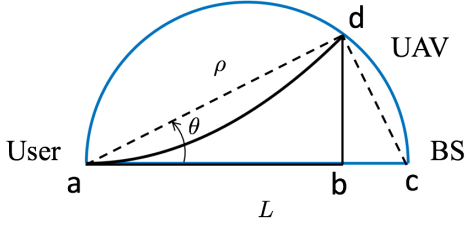


Figure 7. Search region and search trajectory, where point **a** denotes user, point **c** denotes the BS, and point **d** denotes UAV at the boundary of the search area.

which equals to γ , being strictly positive. Therefore, Step 3) strictly increases $\rho(t)$.

In addition, Step 3b) moves on the contour of $F_k(\rho, \theta) = C$, whose dynamics is give by

$$\frac{\partial F_k(\rho, \theta)}{\partial \rho} d\rho + \frac{\partial F_k(\rho, \theta)}{\partial \theta} d\theta = 0$$

in which $\partial F_k(\rho(t), \theta(t))/\partial \rho \leq 0$ according to Lemma 6 (with a straight-forward generalization from F_1 to F_k) and $\partial F_k(\rho, \theta)/\partial |\theta| > 0$ according to Lemma 4. As a result, Step 3b) monotonically increases $|\theta(t)|$. \square

We now show that the boundary of the search region \mathcal{P} in (17) for the $\theta > 0$ branch is given by a semi-circle as illustrated in Fig. 7 (the blue semi-circle). To see this, we first note that the boundary of \mathcal{P} for $\theta > 0$ is given by $(\rho \cos \theta, \rho \sin \theta)$, where $\rho = L \cos \theta$ and $0 \leq \theta \leq \pi/2$. Therefore, $\overline{ad} = L \cos \theta$, $\overline{ac} = L$,

$$\overline{dc} = \sqrt{(L \cos^2 \theta - L)^2 + (L \cos \theta \sin \theta - 0)^2}$$

which yields $(\overline{ad})^2 + (\overline{dc})^2 = (\overline{ac})^2$, and hence point **d** is on the semi-circle with the diameter given by line segment \overline{ac} .

From the monotone property in Lemma 10, the search trajectory is a convex curve starting from point **a** at the user and ending at the semi-circle, e.g., point **d**. Note that the length of any curve \overline{ad} is less than

$$\overline{ab} + \overline{bd} = L \cos^2 \theta + L \cos \theta \sin \theta$$

where the maximum value over $0 \leq \theta < \pi/2$ can be numerically evaluated to be roughly $1.2L$.

Algorithm 1 consists of the search on the BS-user axis with maximum length L , and $K - 1$ loops for the off-BS-user axis searches, where each loop consists of searches on the left and right branches each with maximum length $1.2L$. As a result, the total length of the search trajectory is upper bounded by $(2.4K - 1.4)L$. \blacksquare

REFERENCES

- [1] Y. Zeng, R. Zhang, and T. J. Lim, "Wireless communications with unmanned aerial vehicles: opportunities and challenges," *IEEE Commun. Mag.*, vol. 54, no. 5, pp. 36–42, 2016.
- [2] M. Mozaffari, W. Saad, M. Bennis, and M. Debbah, "Unmanned aerial vehicle with underlaid device-to-device communications: Performance and tradeoffs," *IEEE Trans. Wireless Commun.*, vol. 15, no. 6, pp. 3949–3963, 2016.
- [3] Z. Xiao, P. Xia, and X.-G. Xia, "Enabling UAV cellular with millimeter-wave communication: Potentials and approaches," *IEEE Commun. Mag.*, vol. 54, no. 5, pp. 66–73, 2016.
- [4] B. Van Der Bergh, A. Chiumento, and S. Pollin, "LTE in the sky: trading off propagation benefits with interference costs for aerial nodes," *IEEE Commun. Mag.*, vol. 54, no. 5, pp. 44–50, 2016.
- [5] A. Merwaday and I. Guvenc, "UAV assisted heterogeneous networks for public safety communications," in *Proc. Wireless Commun. and Networking Conf. Workshops*, 2015, pp. 329–334.
- [6] D.-T. Ho, P. Sujit, T. A. Johansen, and J. B. De Sousa, "Performance evaluation of cooperative relay and particle swarm optimization path planning for UAV and wireless sensor network," in *Proc. IEEE Globecom Workshops*, 2013, pp. 1403–1408.
- [7] V. Sharma, M. Bennis, and R. Kumar, "UAV-assisted heterogeneous networks for capacity enhancement," *IEEE Commun. Lett.*, vol. 20, no. 6, pp. 1207–1210, 2016.
- [8] O. Jian, Z. Yi, L. Min, and L. Jia, "Optimization of beamforming and path planning for UAV-assisted wireless relay networks," *Chinese Journal of Aeronautics*, vol. 27, no. 2, pp. 313–320, 2014.
- [9] Y. Jin, Y. D. Zhang, and B. K. Chalise, "Joint optimization of relay position and power allocation in cooperative broadcast wireless networks," in *Proc. IEEE Int. Conf. Acoustics, Speech, and Signal Processing*, 2012, pp. 2493–2496.
- [10] D. H. Choi, B. H. Jung, and D. K. Sung, "Low-complexity maneuvering control of a UAV-based relay without location information of mobile ground nodes," in *Proc. IEEE Symposium on Computers and Commun.*, 2014, pp. 1–6.
- [11] A. Chamseddine, G. Charland-Arcand, O. Akhrif, S. Gagné, F. Gagnon, and D. Couillard, "Optimal position seeking for unmanned aerial vehicle communication relay using only signal strength and angle of arrival," in *IEEE Conf. on Decision and Control*, Dec 2014, pp. 976–981.
- [12] F. Jiang and A. L. Swindlehurst, "Optimization of UAV heading for the ground-to-air uplink," *IEEE J. Sel. Areas Commun.*, vol. 30, no. 5, pp. 993–1005, 2012.
- [13] A. Al-Hourani, S. Kandeepan, and A. Jamalipour, "Modeling air-to-ground path loss for low altitude platforms in urban environments," in *Proc. IEEE Global Telecomm. Conf.*, 2014, pp. 2898–2904.
- [14] M. Mozaffari, W. Saad, M. Bennis, and M. Debbah, "Drone small cells in the clouds: Design, deployment and performance analysis," in *Proc. IEEE Global Telecomm. Conf.*, 2015, pp. 1–6.
- [15] A. Hourani, K. Sithamparanathan, and S. Lardner, "Optimal LAP altitude for maximum coverage," *IEEE Commun. Lett.*, no. 99, pp. 1–4, 2014.
- [16] M. Mozaffari, W. Saad, M. Bennis, and M. Debbah, "Optimal transport theory for power-efficient deployment of unmanned aerial vehicles," in *Proc. IEEE Int. Conf. Commun.*, Kuala Lumpur, Malaysia, May 2016, pp. 1–6.
- [17] —, "Efficient deployment of multiple unmanned aerial vehicles for optimal wireless coverage," *IEEE Commun. Lett.*, vol. 20, no. 8, 2016.
- [18] Q. Feng, J. McGeehan, E. K. Tameh, and A. R. Nix, "Path loss models for air-to-ground radio channels in urban environments," in *Proc. IEEE Semiannual Veh. Technol. Conf.*, vol. 6, 2006, pp. 2901–2905.
- [19] J. Chen and D. Gesbert, "Joint user grouping and beamforming for low complexity massive MIMO systems," in *IEEE Int. Workshop on Signal Process. Advances in Wireless Commun.*, Edinburgh, UK, May 2016, pp. 1–6.
- [20] T. Bai and R. W. Heath, "Coverage and rate analysis for millimeter-wave cellular networks," *IEEE Trans. Wireless Commun.*, vol. 14, no. 2, pp. 1100–1114, 2015.
- [21] J. Chen, U. Yatnalli, and D. Gesbert, "Learning radio maps for UAV-aided wireless networks: A segmented regression approach," in *Proc. IEEE Int. Conf. Commun.*, Paris, France, May 2017.
- [22] J. Chen, O. Esrafilian, D. Gesbert, and U. Mitra, "Efficient algorithms for air-to-ground channel reconstruction in UAV-aided communications," in *Proc. IEEE Global Telecomm. Conf.*, Dec. 2017, Wi-UAV workshop.
- [23] R. U. Nabar, H. Bolcskei, and F. W. Kneubuhler, "Fading relay channels: Performance limits and space-time signal design," *IEEE J. Sel. Areas Commun.*, vol. 22, no. 6, pp. 1099–1109, 2004.
- [24] J. N. Laneman, D. N. Tse, and G. W. Wornell, "Cooperative diversity in wireless networks: Efficient protocols and outage behavior," *IEEE Trans. Inf. Theory*, vol. 50, no. 12, pp. 3062–3080, 2004.
- [25] T. Wang, A. Cano, G. B. Giannakis, and J. N. Laneman, "High-performance cooperative demodulation with decode-and-forward relays," *IEEE Trans. Commun.*, vol. 55, no. 7, pp. 1427–1438, 2007.
- [26] "Winner II interim channel models," Tech. Rep. IST-4-027756 WINNER II D1.1.2 v1.2, Sept. 2007.